Nanoscale Structure Formation on Sputter Eroded Surface

B. Kahng*

Center for Theoretical Physics and School of Physics, Seoul National University, Seoul 151-742

H. Jeong and A-L. Barabási

Department of Physics, University of Notre Dame, Notre Dame, IN 46556, U.S.A.

We investigate the morphological features of sputter eroded surfaces, demonstrating that while at short times ripple formation is described by the linear theory, after a characteristic time, the nonlinear terms determine the surface morphology, by monitoring the surface width and the erosion velocity. Furthermore, we show that sputtering under normal incidence leads to the formation of spatially ordered uniform nanoscale islands or holes. We find that while the size of these nanostructures is independent of flux and temperature, it can be controlled by ion beam energy.

I. INTRODUCTION

Experimental results on ion sputtered surfaces, covering amorphous and crystalline materials (SiO_2 [1]), and both metals (Ag [2]) and semiconductors (Ge [3], Si [4,5]), have motivated extensive theoretical work aiming to uncover the mechanism responsible for ripple formation and kinetic roughening. A particularly successful model has been proposed by Bradley and Harper (BH) [6], in which the height $h(x,y,t)$ of the eroded surface is described by the linear equation

$$\partial_t h = \nu_x \partial_x^2 h + \nu_y \partial_y^2 h - K \partial^4 h, \qquad (1)$$

where ν_x and ν_y are effective surface tensions, and K is the surface diffusion constant. The balance of the unstable erosion term $(-|\nu|\partial^2 h)$ and the smoothing surface diffusion term $(-K\partial^4 h)$ generates ripples with wavelength $\ell_i = 2\pi\sqrt{2K/|\nu_i|}$, where i refers to the direction (x or y) along which the associated ν_i (ν_x or ν_y) is the largest. While successful in predicting the ripple wavelength and orientation [7], this linear theory cannot explain a number of experimental features, such as the saturation of the ripple amplitude [8–10], the observation of rotated ripples [11], and the appearance of kinetic roughening [12,13]. These phenomena can be explained by the noisy nonlinear equation, called the Kuramoto-Sivashinsky (KS) equation [14],

$$\partial_t h = \nu_x \partial_x^2 h + \nu_y \partial_y^2 h - K_x \partial_x^4 h - K_y \partial_y^4 h$$
$$-K_{xy}\partial_x^2\partial_y^2 h + \frac{\lambda_x}{2}(\partial_x h)^2 + \frac{\lambda_y}{2}(\partial_y h)^2 + \eta(x,y,t), \quad (2)$$

where λ_x and λ_y describe the tilt-dependent erosion rate, and $\eta(x,y,t)$ is an uncorrelated white noise with zero mean, and mimicks the randomness resulting from the stochastic nature of ion arrival to the surface [14,15].

When the nonlinear terms and the noise are neglected, Eq.(2) reduces to the linear theory Eq. (1), and predicts ripple formation. It is known that the isotropic KS equation ($\nu_x = \nu_y < 0$, $K_x = K_y = K_{xy}/2$, and $\lambda_x = \lambda_y$) asymptotically (for large time and length scales) predicts kinetic roughening, with exponents similar to those seen experimentally in ion sputtering [12]. For positive ν_x and ν_y, Eq. (2) reduces to the anisotropic Kardar-Parisi-Zhang (KPZ) equation [16], whose scaling behavior is controlled by the sign of $\lambda_x \cdot \lambda_y$ [17]. Finally, a recent integration by Rost and Krug [18] of the noiseless version of Eq. (2) provided evidence that when $\lambda_x \cdot \lambda_y < 0$, new ripples, unaccounted for by the linear theory, appear and that their direction is rotated with respect to the ion direction [18]. The nonlinear effects have been largely unexplored experimentally due to lack of theoretical predictions of an experimentally detectable signature that distinguishes them from the linear effects. To make specific predictions on the morphology of ion-sputtered surfaces, we need to gain a full understanding of the nonlinear behavior predicted by Eq. (2). In this paper we numerically integrate Eq. (2), aiming to uncover the dynamics and the morphology of the surfaces for different values of the parameters.

II. SIMULATIONS

The direct numerical integration is carried out by using standard discretization techniques to discretize the
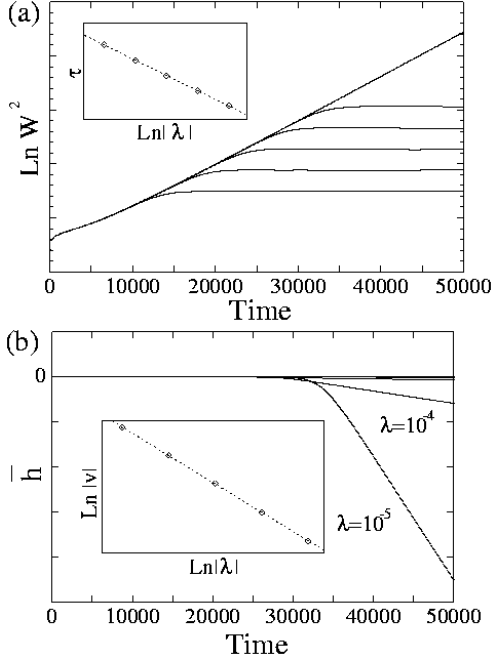
*E-mail: kahng@phya.snu.ac.kr

Fig. 1. Time evolution of (a) the surface width W^2 and (b) the mean height $\bar{h}$ for the parameters $\nu_x = -0.0001$, $\nu_y = -0.6169$, and $K_x = K_y = K_{xy}/2 = 2$. The different curves correspond to different values of $\lambda_x = \lambda_y = \lambda$. In (a), from top to bottom, the curves correspond to $\lambda = 0$, -10^{-5}, -10^{-4}, -10^{-3}, -10^{-2}, and -10^{-1}, respectively. In (b), from bottom to top, they correspond to $\lambda = -10^{-5}$, -10^{-4}, -10^{-3}, -10^{-2}, and -10^{-1}, respectively. Inset (a): The crossover time τ, estimated from (a) is shown as a function of $\ln|\lambda|$. Inset (b): Plot of $\ln|v|$ versus $\ln|\lambda|$. The dotted line has a slope ≈ -1.07, implying $v \sim 1/\lambda$.

continuum equation, Eq. (2) [19]. Since the sign of the nonlinear terms plays a significant role in defining the surface morphology, we discuss separately the $\lambda_x \cdot \lambda_y > 0$ and $\lambda_x \cdot \lambda_y < 0$ cases.

The $\lambda_x \cdot \lambda_y > 0$ case: A general feature of systems such as Eq. (2) is that the nonlinear terms do not affect the surface morphology or dynamics until a crossover time τ has been reached. Thus, we expect that for early times, *i.e.*, for $t < \tau$, the surface morphology and dynamics are properly described by the linear theory. To demonstrate this separation of the linear and nonlinear regions, in Fig. 1, we show the time dependences of the surface width defined as $W^2(L, t) \equiv \frac{1}{L^2} \sum_{x,y} h^2(x, y, t) - \bar{h}^2$ and of the mean height $\bar{h} = \frac{1}{L^2} \sum_{x,y} h(x, y, t)$. We find that for $t < \tau$, the width W increases exponentially while the mean height stays constant at $\bar{h} = 0$. Furthermore, inspecting the surface morphology, we find that in this region the ripple wavelength and orientation are also correctly described by the linear theory.

While the early time behavior is correctly predicted by the linear theory, beyond the crossover time τ, the nonlinear terms become effective. One of the most striking
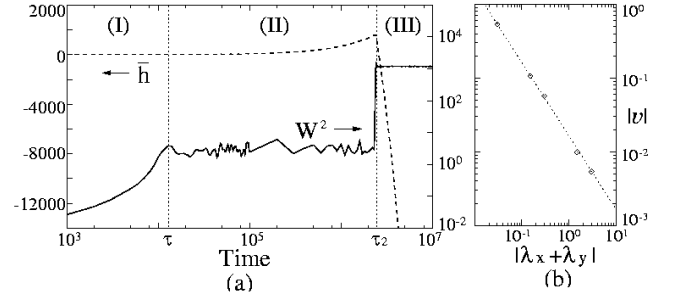

Fig. 2. (a) Time evolution of the mean height $\bar{h}$ (dashed, left linear scale) and the surface width (solid, right logarithmic scale) for the parameters, $\nu_x = -0.6169$, $\nu_y = -0.01$, $K_x = K_y = K_{xy}/2 = 2$, $\lambda_x = 1$, and $\lambda_y = -4$. The dotted lines seperate the three regions discussed in the text. (b) The dependence of $|v|$ on the nonlinear terms $|\lambda_x + \lambda_y|$ for the same parameters used in (a). The dotted line has a slope ≈ -1.02, implying $v \sim 1/(\lambda_1 + \lambda_2)$.

consequence of these terms is that the surface width stabilizes rather abruptly [see Fig. 1]. Furthermore, the ripple pattern generated in the linear region disappears, and the surface exhibits kinetic roughening. The crossover time τ from the linear to the nonlinear behavior can be estimated by comparing the strength of the linear term with that of the nonlinear term [20]:

$$\tau \sim (K/\nu^2) \ln(\nu/\lambda). \tag{3}$$

In this expression, ν, K, and λ refer to the direction perpendicular to the ripple orientation. The predicted λ-dependence of τ is confirmed in the inset of Fig. 1(a). Another quantity that refects the transition from the linear to the nonlinear region is the erosion velocity $v = \partial_t \bar{h}$. The nonlinear terms act to decrease the mean height in the case of $\lambda_x < 0$ and $\lambda_y < 0$. We can estimate the surface velocity as $v \sim \lambda W(L, \tau)^2/\ell^2 \sim \nu^3/(K\lambda)$ using $W(L, \tau) \sim \nu/\lambda$. This dependence of v on λ is consistent with the numerical results shown in the inset of Fig. 1(b).

The $\lambda_x \cdot \lambda_y < 0$ case: As Fig. 2(a) shows, we again observe a separation of the linear and the nonlinear regions; however, we find that the morphology and the dynamics of the surface in the nonlinear region are quite different from the case $\lambda_x \cdot \lambda_y > 0$. In region I, for early times $(t < \tau)$, the surface forms ripples whose wavelength and orientation is correctly described by the linear theory. After the first crossover time τ, given by Eq. (3), the surface width is stabilized, and the ripples disappear. After τ, the system enters a rather long transient region, that we call region II. Here, the surface is rough, and no apparent spatial order is present. We often observe the development of individual ripples, but they soon disappear, and no long-range order is present in the system. However, at a second crossover time, τ_2, a new ripple structure suddenly forms, in which the ripples are stable and rotated with an angle θ_c to the x direction. The angle θ_c has the value $\theta_c = \tan^{-1} \sqrt{-\lambda_x/\lambda_y}$, (or
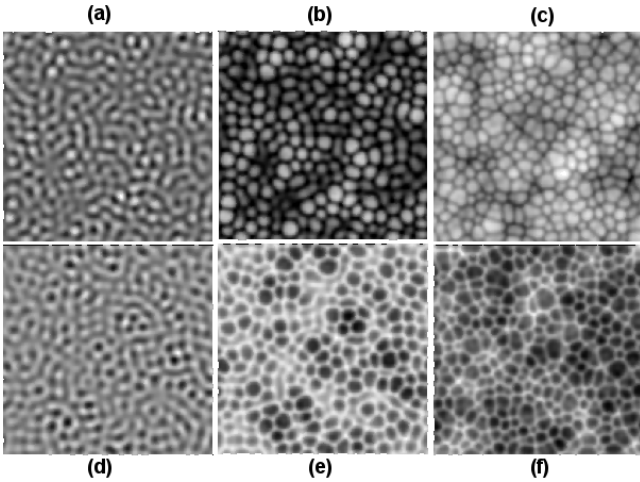
Fig. 3. (a) − (c) Surface morphologies predicted by Eq. (2) for $\lambda = 1$ at different stages of surface evolution. The pictures correspond to (a) $t = 4.0$, (b) 5.8, and (c) 8.0×10^4. (d) − (f) are the same as in (a) − (c), but for $\lambda = -1$. In all cases, we used $\nu = 0.6169$, $K = 2$, and a system size 256×256.

$\tan^{-1} \sqrt{-\lambda_y/\lambda_x}$) [18].

The demonstrated morphological transitions generate an anomalous behavior in $\bar{h}$ as well. As Fig. 2(a) shows, the mean height is zero in the linear region, increases as the ripples are destroyed in region II, and decreases with a constant velocity in region III. More specifically, ripples are aligned along the y-axis in region I, because $\ell_x \ll \ell_y$. Thus, the contribution of $(\partial_x h)^2$ is much larger than that of $(\partial_y h)^2$, even though $|\lambda_x| < |\lambda_y|$, and the surface height increases due to the term $\lambda_x(\partial_x h)^2$ with $\lambda_x > 0$ in region II. However, as the ripples are destroyed by the nonlinear effects, the contribution of the $(\partial_y h)^2$ term increases, and eventually $\lambda_y(\partial_y h)^2$ becomes larger than $\lambda_x(\partial_x h)^2$, forcing the mean height to decrease because $\lambda_y < 0$. The velocity in region III is determined by the nonlinear coefficient in the direction along the ripples, which reduces to $\lambda_x + \lambda_y$ after a coordinate transformation to the rotated ripple direction. This prediction is in good agreement with the results of Fig. 2(b), which demonstrates that $v \sim 1/(\lambda_x + \lambda_y)$.

III. QUANTUM DOT AND HOLE FORMATION

Under normal incidence [21], the coefficients in Eq.(2) are isotropic and are given by [15,22]

$$\nu \equiv \nu_x = \nu_y = -faa_\sigma^2/2a_\mu^2, \qquad (4)$$

$$K \equiv K_x = K_y = fa^3 a_\sigma^2/8a_\mu^4, \qquad (5)$$

$$\lambda \equiv \lambda_x = \lambda_y = (f/2a_\mu^2)(a_\sigma^2 - a_\sigma^4 - a_\mu^2), \qquad (6)$$

where $a_\mu = a/\mu$ and $a_\sigma = a/\sigma$, and μ and σ characterize the shape of the collision cascade of the bombard-

ing ion. The morphology of the ion-sputtered surface at three different stages of time evolution is shown in Fig. 3. Let us first concentrate on the $\lambda > 0$ case [upper panels in Fig. 3]. In the early stages of the sputtering process, the surface is dominated by small, wavy perturbations [Fig. 3(a)] generated by the interplay between the ion-induced instability and surface relaxation. However, since the system is isotropic in the (x, y) plane, these ripple precursors are oriented randomly, generating short wormlike morphologies on the surface. After some characteristic time, τ, these structures turn into isolated but closely packed islands, reminiscent of the quantum dots (QDs) reported experimentally [Fig. 3(b)] [23]. Note that upon a closer inspection one can observe the emergence of hexagonal order in the island positions. As the sputtering proceeds, the supporting surface develops a rough profile, destroying the overall uniformity of the islands [Fig. 3(c)]. A similar scenario is observed for $\lambda < 0$, the only difference being that now the islands are replaced by holes [Figs. 3(d) − (f)]. The first conclusion we can draw from these results is that the development of QDs and holes is governed by the same underlying physical phenomena, the only difference being that for QDs we have $\lambda > 0$, and for holes $\lambda < 0$. Indeed, this morphological change is expected from the nonlinear continuum theory, Eq. (2), being symmetric under the simultaneous transformation $\lambda \to -\lambda$ and $h \to -h$, indicating that changing the sign of λ does not affect the dynamics of the surface evolution, but simply turns the islands into mirrored holes. Since, according to Eq. (5) the sign of λ is determined only by the relative magnitudes of a_σ and a_μ, whether islands or holes appear is determined by the shape of the collision cascade [21]. Consequently, using Eq. (5) we can draw a phase diagram in terms of the reduced penetration depths, a_σ and a_μ, that separate the regions displaying QDs and holes [21]. These results also indicate that the QDs and holes are inherently nonlinear objects, since, should the linear terms be responsible for their formation, the surface morphology should not depend on the sign of λ (Eq. (1) has a full $h \to -h$ symmetry.)

Using Eqs. (3) and (4), we find that $\ell = \sqrt{2}\pi\mu$; *i.e.*, from the average separation of the islands one can determine the size of the horizontal width of the collision cascade [21]. Furthermore, since typically we have $\mu \sim a \sim \epsilon^{2m}$, when ϵ is the ion energy and m is an constant that weakly depend on ϵ ($m = 1/2$ for $\epsilon \approx 10 \sim 100$ keV), we predict that one can tune the size of the QDs by changing the ion energy ϵ, while the size is independent of the flux and the temperature. It would be interesting to reproduce surface morphology using numerical simulations directly [24].

REFERENCES

[1] T. M. Mayer, E. Chason and A. J. Howard, J. Appl. Phys. **76**, 1633 (1994).

[2] S. Rusponi, C. Boragno and U. Valbusa, Phys. Rev. Lett. **78**, 2795 (1997).

[3] E. Chason, T. M. Mayer, B. K. Kellerman, D. T. McIlroy and A. J. Howard, Phys. Rev. Lett. **72**, 3040 (1994).

[4] G. Carter and V. Vishnyakov, Phys. Rev. B **54**, 17647 (1996); Z. X. Jiang and P. F. A. Alkemade, Appl. Phys. Lett. **73**, 315 (1998).

[5] J. Erlebacher, M. J. Aziz, E. Chason, M. B. Sinclair and J. A. Floro, Phys. Rev. Lett. **82**, 2330 (1999).

[6] R. M. Bradley and J. M. E. Harper, J. Vac. Sci. Technol. A **6**, 2390 (1988).

[7] I. Koponen, M. Hautala and O-P. Sievaenen, Phys. Rev. Lett. **78**, 2612 (1997).

[8] K. Wittmaack, J. Vac. Sci. Technol. A **8**, 2246 (1990).

[9] J. Erlebacher, M. J. Aziz, E. Chason, M. B. Sinclair and J. A. Floro, J. Vac. Sci. Technol. A **18**, 115 (2000).

[10] J. J. Vajo, R. E. Doty and E-H. Cirlin, J. Vac. Sci. Technol. A **6**, 76 (1988).

[11] S. Rusponi, G. Costantini, C. Boragno and U. Valbusa, Phys. Rev. Lett. **81**, 2735 (1998).

[12] E. A. Eklund, R. Bruinsma, J. Ruidnick and R. S. Williams, Phys. Rev. Lett. **67**, 1759 (1991).

[13] H-N. Yang, G-C. Wang and T-M. Lu, Phys. Rev. B **50.** 7635 (1994).

[14] R. Cuerno and A-L. Barabási, Phys. Rev. Lett. **74**, 4746 (1995).

[15] M. A. Makeev and A-L. Barabási, Appl. Phys. Lett. **71**, 2800 (1997).

[16] M. Kardar, G. Parisi and Y-C. Zhang, Phys. Rev. Lett. **56**, 889 (1986).

[17] D. E. Wolf, Phys. Rev. Lett. **67**, 1783 (1991).

[18] M. Rost and J. Krug, Phys. Rev. Lett. **75**, 3894 (1995).

[19] W. H. Press, B. P. Flannery, S. A. Teukolsky and W. T. Vetterling, *Numerical Recipes* (Cambridge Univ. Press, Cambridge, 1986).

[20] S. Park, B. Kahng, H. Jeong and A.-L. Barabási, Phys. Rev. Lett. **83**, 3486 (1999).

[21] B. Kahng, H. Jeong and A.-L. Barabási, Appl. Phys. Lett. **78**, 805 (2001).

[22] M. Makeev, R. Cuerno and A.-L. Barabási (preprint).

[23] S. Facsko, T. Dekorsy, C. Koerdt, C. Trappe, H. Kurz, A. Vogt and H. L. Hartnagel, Science **285**, 1551 (1999).

[24] Y. Ban, T. Won and J. Lee, J. Korean Phys. Soc. **35**, S829 (1999).